Available online at www.sciencedirect.com
SCIENCE DIRECT®
Catalysis Today 89 (2004) 47–55
CATALYSIS TODAY
www.elsevier.com/locate/cattod

Diagnosis of atmospheric pressure low temperature plasma and application to high efficient methane conversion

Shigeru Kado [a,*], Yasushi Sekine [b], Tomohiro Nozaki [a], Ken Okazaki [a]

[a] *Department of Mechanical and Control Engineering, Graduate School of Science and Engineering, Tokyo Institute of Technology, 2-12-1 O-okayama, Meguro-ku, Tokyo 152-8552, Japan*
[b] *Department of Applied Chemistry, School of Science and Engineering, Waseda University, Okubo, Shinjuku-ku, Tokyo 169-8555, Japan*

Abstract

Direct dehydrogenation of methane to produce more useful chemicals was examined using low temperature plasmas such as DBD, corona and spark discharge under the conditions of room temperature and atmospheric pressure. In spark discharge, acetylene was produced with the selectivity higher than 85% and small amount of deposited carbon. The energy efficiency in spark discharge was much higher than that in DBD and corona discharge. By the emission spectroscopy, it was found that methane was highly dissociated to atomic carbon and hydrogen in spark discharge. The gas temperature in spark discharge channel remained as low as 420–460 K determined by Boltzmann plot method of CH rotational band (431 nm). The specific energy requirement for acetylene was improved by the optimization of reactor size and residence time and reached 12.1 kW h/kg-C_2H_2, which was as same as Huels process with DC arc plasma.

Keywords: Methane; Acetylene; Spark discharge; Optical emission spectroscopy; Gas temperature; Energy efficiency

1. Introduction

From a point of view of chemical utilization of natural gas, methane conversion into valuable products such as hydrogen, synthesis gas, C_2 and higher hydrocarbons has been examined under various conditions. The activation of methane requires a high reaction temperature due to its thermal stability. Even in the industrial process to produce hydrogen by steam reforming, the operating temperature is higher than 1073 K in the presence of catalysts. The higher temperature is favorable for promoting the reaction, but is not suitable for the selective formation of ethane/ethylene and oxygen-containing liquid compounds by oxidative coupling and partial oxidation. That is one of the reasons why the high yield of these products, sufficient for the commercialization, has not been obtained [1].

To resolve these problems, we have paid attention to the low temperature plasma having a property of high electron temperature and low gas phase temperature, and succeeded in the formation of acetylene with high yield at ambient temperature in gas phase homogeneous reaction using the spark discharge [2]. The formation of synthesis gas by carbon dioxide or steam reforming and partial oxidation was also examined with and without catalyst [3–5]. Recently, the conversion of methane using non-equilibrium plasmas has attracted a considerable attention in the field of reforming as well as deposition of carbon materials. Nozaki et al. have succeeded in the growth of carbon nanotubes with atmospheric pressure glow discharge (APG) [6], and Liu et al. deposited the diamond-like carbon film using dielectric barrier discharge (DBD) [7]. Many researches of DBD conversion of methane into more useful chemicals including synthesis gas, gaseous and liquid hydrocarbons and oxygenates have been done [8–12], and recently it was found that the use of starch significantly increases the selectivity to oxygenates [12]. Steam reforming of methane was investigated using ferroelectric packed-bed reactor [13], and microwave reforming of methane with carbon dioxide has been examined [14,15]. The microwave plasma has also been reported to be useful for the selective formation of acetylene [16–18].

In this work, the reactivity and the energy efficiency of the spark discharge were compared with those of other cold plasmas such as dielectric barrier discharge (DBD) and corona discharge. The emission spectroscopic diagnostics of the spark discharge was also done to know the gas phase temperature in the discharge channel and active species. In addition,

* Corresponding author. Tel.: +81-3-5734-2179; fax: +81-3-5734-2893.
E-mail address: k-shigeru@kit.hi-ho.ne.jp (S. Kado).

0920-5861/$ – see front matter © 2003 Elsevier B.V. All rights reserved.
doi:10.1016/j.cattod.2003.11.036

the energy efficiency for the production of acetylene was improved by the optimization of reaction conditions.

2. Experimental

2.1. Reaction apparatus

The differences of the reactivity including the conversion, products selectivity and energy efficiency among DBD, corona and spark discharge were examined with the reactors as shown in Fig. 1. A flow type reactor composed of a quartz tube with 16.5 mm i.d. and 19.5 mm o.d. (1.5 mm thickness) was used through the all experiments under the conditions of room temperature and atmospheric pressure without any catalysts. The reactant was a 99.9999% purity of methane, of which flow rate was controlled with a thermal mass flow controller. In this study, the effect of the residence time was investigated by varying the flow rate under the same discharge conditions.

In DBD, the electrodes configuration was the coaxial type as shown in Fig. 1(a). Inside of the reactor, the high voltage electrode of copper with 14.5 mm o.d. was inserted and fixed at the center. The outside of the reactor was covered with aluminum tape and grounded. The quartz glass of the reactor played a role of the dielectric material. The gap distance and the length of the discharge region were 1.0 and 40 mm, which corresponded to 2.0 cm^3 volume of the discharge region. AC high voltage with 75 kHz frequency was applied between the electrodes, and the supplied discharge power was fixed at 17 W, which was determined from a voltage–charge diagram called a Lissajous figure. To reduce the effect of electrical noises, we used the averaged Lissajous figure over 16 times sampling.

In corona and spark discharge, the same reactor was used as shown in Fig. 1(b). The electrodes configuration was needle to needle type. The stainless steel rods with Ø1 mm were used as the electrodes. The electrodes were centered and supported with the stainless steel mesh with 5.0 mm gap distance. DC negative high voltage was applied between the electrodes. In corona discharge, 1 MΩ high voltage resistor was inserted between the power supply and the electrode. The corona current was estimated from the decrease in the voltage at the resistor, and the discharge power was fixed at

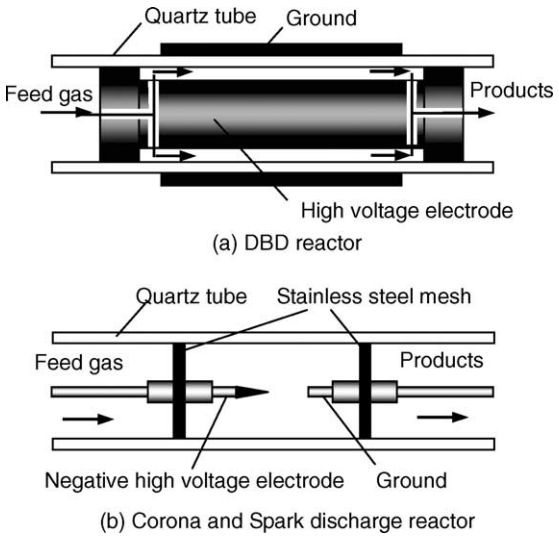

Fig. 1. Schematic diagram of reactors.

4.6 W. The details of DC power supply and the spark discharge are described later.

2.2. DC high voltage power supply

Fig. 2 shows the schematic diagram of DC high voltage power supply used in this study. The leakage transformer (1:150, 140 VA) produced high voltage from AC voltage of 50 Hz. AC high voltage was rectified with the diode, and the capacitor C_1 (36,000 pF) was charged through the resistor R_1 (1 kΩ). In this study, the negative voltage was employed. This circuit provided the stable DC high voltage (15 kV capacity), and the capacitor C_2 (1410 pF) was charged through resistor R_2 (100 kΩ). The discharge current was supplied to the reactor through resistor R_3 (100 Ω). The stable pulsed discharge was obtained due to the relationship of the time constant of $R_2C_2 \gg R_3C_2$. In the spark discharge, discharge voltage was measured at the end of the resistor R_3, and the current was measured at the ground.

2.3. Properties of spark discharge

Fig. 3 shows the waveforms of voltage and current in spark discharge measured with a digital oscilloscope under the

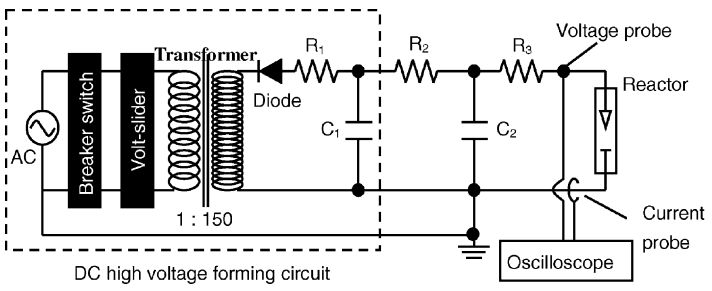

Fig. 2. Schematic diagram of DC high voltage power supply.

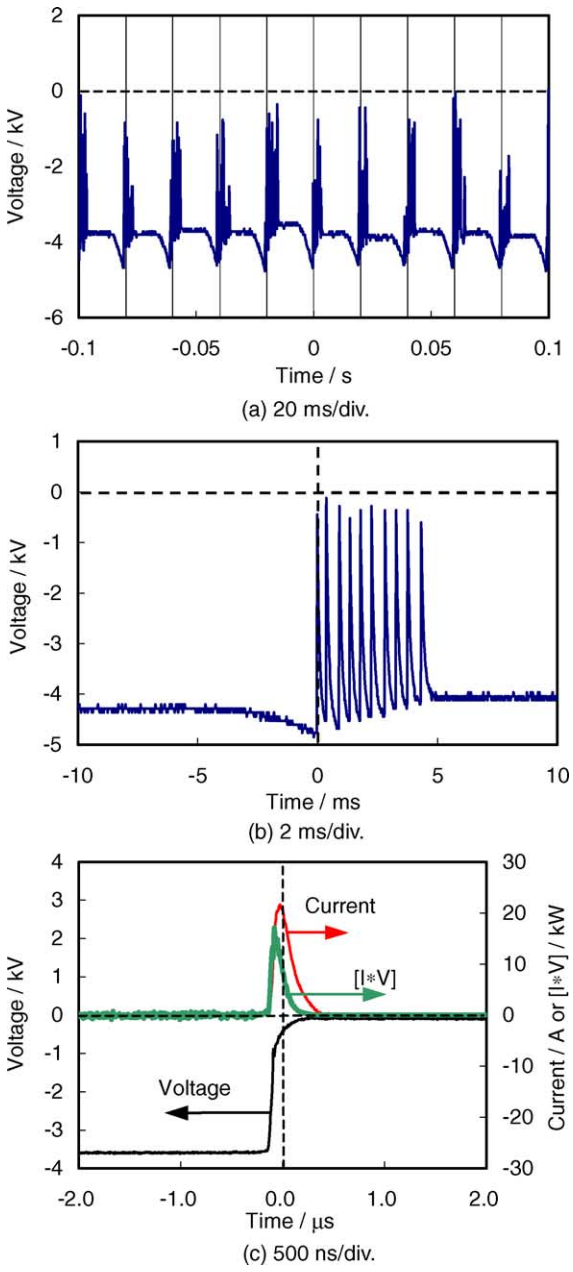

Fig. 3. Waveforms of voltage and current of spark discharge.

conditions of 5 mm gap distance and methane flow. The intermittent spark discharge occurred periodically with 50 Hz pulse frequency (20 ms pulse period) and ca. −5 kV inception voltage as shown in Fig. 3(a). From the detail measurement of voltage of one pulse (shown in Fig. 3(b)), it was clear that there were a dozen of spikes at one pulse. The number of spikes at a pulse was uncertain and distributed from 5 to 19 spikes as shown in Fig. 4. From Fig. 4, the average number of spikes was decided to be 12.6 spikes per pulse.

The waveforms of voltage and current in one spike were shown in Fig. 3(c), which were averaged over 16 times sampling. The voltage recovered to 0 V in a few hundreds of nanoseconds, and the pulsed current occurred. The pulsed

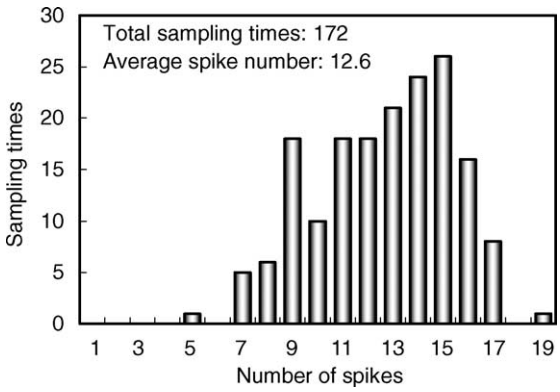

Fig. 4. Histogram of the number of spikes at a pulse.

current reached 20–30 A with a width of 300–500 ns. This short width of current contributed to non-equilibrium plasma having characteristics of extremely high electron temperature and low gas phase temperature.

From Fig. 3(c), the discharge energy at a spike (P_S) was defined as follows:

$$P_S = \sum_i \frac{(|V_i \times I_i| + |V_{i+1} \times I_{i+1}|) \times (t_{i+1} - t_i)}{2}$$

Total energy injection rate of spark discharge (P) in watts was defined as follows from P_S, average number of spikes (N_S) and pulse frequency (F):

$$P = P_S N_S F$$

In this study, spark discharge power was fixed at 1.4 W under standard condition.

2.4. Analysis

The waveforms of applied voltage and current were measured with the digital oscilloscope (Tektronix TDS644A, 500 MHz band width, 2 G samples/s maximum sampling rate) using voltage probe (Tektronix P6015A, 75 MHz band width, 1000:1) and current probe (Tektronix P6021, 60 MHz band width, 10:1). The gaseous products were analyzed by gas chromatography equipped with FID (G-950 column and Porapk N column) and TCD (SHIN-carbon column).

In DBD and spark discharge, the effluent gas was analyzed at least three times during plasma reaction time of 1 h. It was confirmed that the experiment has already reached steady state after 5 min from discharge on. In corona discharge, the sampled data of 5 min after discharge on were employed to reduce the effect of a large amount of deposited carbon.

The amount of deposited carbon was estimated from the total amount of CO and CO_2 in the combustion of deposited materials in the air at 923 K. The conversion of methane was defined as follows:

$$\text{methane conversion} = \frac{\text{moles of methane consumed}}{\text{moles of methane introduced}} \times 100\%$$

The selectivities of products were defined as follows:

$$\text{product selectivity} = \frac{\text{carbon based moles of product}}{\text{moles of methane consumed}} \times 100\%$$

The deposited materials were also characterized by Raman spectroscopy (Green laser 532 nm).

For emission spectroscopy, a standard quartz lens was used to maintain the correct focus on the discharge channel. The emission from the discharge region was continuously recorded with an ICCD camera (Andor DH734-18U-03 iStar camera) with 50 ms exposure through an optical fiber, and a 500 mm spectrometer (Acton Research Spectra, Pro 500i) with 1200 grating was used.

3. Results and discussion

3.1. Reactivity of low temperature plasmas

The reactivity of spark discharge was compared with that of DBD and corona discharge in methane flow. Methane conversion and products selectivity were shown in Fig. 5. The experiments were conducted under almost the same conversion, and the conversion was controlled with the operation of flow rate. Methane flow rate was 15 and 30 $cm^3\,min^{-1}$, and the condition of 6 $cm^3\,min^{-1}$ was added in corona discharge reaction. The product of others shown in Fig. 5 was considered to be liquid hydrocarbons higher than C_5.

In DBD, the oligomerization to hydrocarbons higher than C_3 was the main reaction, and the main component in C_2 hydrocarbons was ethane, which was considered formed by the coupling of CH_3 radicals. The selectivity to deposited carbon was as low as 3%. It is necessary to improve the rector design and reaction system to obtain the desired product selectively in DBD reaction.

In corona discharge, although the formation of C_2 hydrocarbons was predominant, the distribution among ethane, ethylene and acetylene was wide and almost equally. In addition, the consecutive dehydrogenation from ethane to ethylene, and further to acetylene was observed with the increase in methane conversion due to high gas phase temperature. The detail of the estimation of gas phase temperature is discussed later. The behavior of the selectivity to deposited carbon was characteristic to corona discharge. With the increase in methane conversion, the amount of deposited carbon drastically increased. The selectivity to carbon increased from 5% at 4% methane conversion to 34% at 25%. The carbon was deposited mainly on the tip of the cathode and grew along the discharge channel. Finally, the deposited carbon made a short circuit between two electrodes.

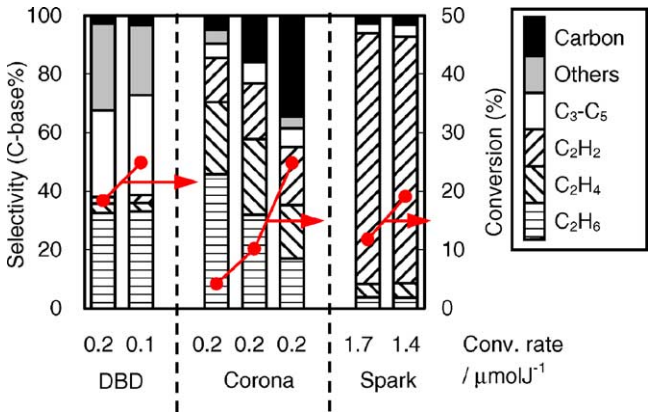

Fig. 5. Comparison of reactivities among DBD, corona and spark discharge in pure methane flow.

On the other hand, in spark discharge, acetylene was produced with the selectivity of 85%. The selectivity did not depend on the conversion. The amount of deposited carbon was small, and the selectivity to carbon was as low as 3%.

The comparison of reactivity among these three types of low temperature plasmas was made using methane conversion rate (R, μmol/J) defined by Yao et al. [19], which is also shown in Fig. 5:

$$R = \frac{\text{moles of methane converted per second}}{P}$$

The amount of deposited carbon is included in moles of methane converted.

Methane conversion rates in DBD and corona discharge were almost the same at 0.2 μmol/J, while the spark discharge reaction showed the high reactivity of 1.7 μmol/J. The reactivity of spark discharge was much higher that that of DBD and corona discharge. When the energy efficiency is taken into consideration, these differences become more conspicuous because the formation of acetylene from methane is highly endothermic reaction compared to that of ethane and ethylene:

$$CH_4 \rightarrow \tfrac{1}{2}C_2H_6 + \tfrac{1}{2}H_2, \quad \Delta H^\circ = 32.5\,\text{kJ/mol},$$
$$CH_4 \rightarrow \tfrac{1}{2}C_2H_4 + H_2, \quad \Delta H^\circ = 101\,\text{kJ/mol},$$
$$CH_4 \rightarrow \tfrac{1}{2}C_2H_2 + \tfrac{3}{2}H_2, \quad \Delta H^\circ = 188\,\text{kJ/mol}$$

Even if only the formation of acetylene was taken into account, the energy efficiency of spark discharge in the case of 1.7 μmol/J conversion rate reached 27%:

$$\text{energy efficiency} = \frac{\Delta H(376\,\text{J/mmol}) \times (\text{formation rate of } C_2H_2\ (\text{mmol s}^{-1}))}{P\ (\text{J s}^{-1})} \times 100\%$$

So, the energy efficiency will be improved when the spark discharge was applied to more highly endothermic reaction such as the reforming to produce synthesis gas and/or hydrogen:

$$CH_4 + H_2O\,(g) \rightarrow CO + 3H_2, \quad \Delta H^\circ = 206\,\text{kJ/mol},$$
$$CH_4 + CO_2 \rightarrow 2CO + 2H_2, \quad \Delta H^\circ = 247\,\text{kJ/mol}$$

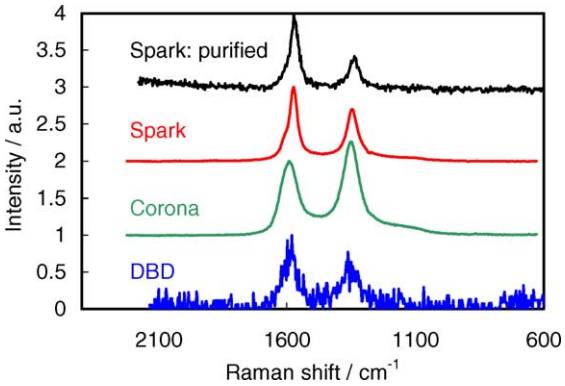

Fig. 6. Raman spectra of deposited carbon materials in DBD, corona and spark discharge.

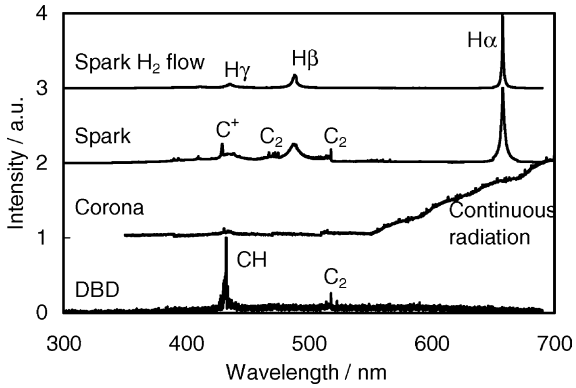

Fig. 7. Emission spectra of DBD, corona and spark discharge in pure methane flow and that of spark discharge in pure hydrogen flow.

When the spark discharge is considered for acetylene synthesis process, the specific energy required to produce 1 kg acetylene is 14.6 kW h/kg-C_2H_2.

3.2. Deposited carbon materials

Fig. 6 shows Raman spectra of the deposited carbon materials obtained in the each plasma. The G-band located around 1580 cm^{-1} attributes C–C stretching vibration of graphite layers, and imperfect graphite structure is characterized from the D-band near 1350 cm^{-1}. The intensities of these G- and D-bands from carbon materials obtained in DBD were weak, which was like tar. The D/G-band intensity ratio of the sample obtained in spark discharge was 0.7, which was lower than that in corona discharge of 1.3. Tohji et al. have developed a purification method and succeeded in obtaining 95 wt.% purity of single-wall nanotubes from the soot produced by arc discharge with Ni and Fe containing graphite electrode [20,21]. In spark discharge, there should be no catalyst metals contained in deposited carbon, only the oxidative removal of the amorphous carbon was employed. The soot obtained in spark discharge was oxidized in H_2O_2 solution for 4 h at 373 K. The D/G-band intensity ratio became lower to 0.3, but the existence of carbon nanotubes was not confirmed by FE-SEM examination.

3.3. Emission spectroscopy

Fig. 7 shows the emission spectra measured in DBD, corona and spark discharge in methane flow. The spectrum obtained in spark discharge in hydrogen flow is also shown in Fig. 7. They were quite different among these three types of low temperature plasmas. The rotational band of 431.5 nm due to an $A^2\Delta - X^2\Pi$ (0, 0) transition had the highest intensity in DBD. The low intensity of emission derived from C_2 swan band system (517 nm, $d^3\Pi_g - a^3\Pi_u$ (0, 0)) was observed. In corona discharge, the emission intensity of CH rotational band was almost the same as that of C_2 swan band system. The continuous radiation was observed in corona discharge, which was cause by carbon deposition in discharge channel.

In spark discharge, the emission intensity of CH rotational band was relatively low, while the strong emission of C_2 swan band system and atomic carbon (C^+, 427 nm) was observed. In addition, when the spectra in methane flow are compared with those obtained in hydrogen flow, it is clear that almost the same spectra of H Balmer series were observed. These facts of the strong intensity of atomic spectra of carbon and H Balmer series in methane flow indicate that methane was highly dissociated into C and H by the electron impact. These results are consistent with the previous work investigating the reaction mechanism using isotopes [5].

3.4. Estimation of gas temperature in discharge channel

There have been many emission spectroscopic methods reported to determine the gas temperature. The Boltzmann plot method can be applied for plasmas in thermodynamic equilibrium, but also in less restrictive conditions, if the pressure is sufficiently high, so that the collisional frequency of the molecules is much higher than the radiative decay probability of the excited state under consideration, resulting in the thermal equilibration of the state populations.

Heintze et al. showed that the rotational temperature determined from C_2 swan band agreed with that determined from H_2 Fulcher-α band using the rotational energy in the ground state between 1500 and 2500 K in a pulsed microwave plasma [18]. On the other hand, when the determination of gas temperature from C_2 swan band was applied to DBD, Pellerin et al. obtained abnormally high temperature of 2970 K, which was much higher than the $T^r_{(OH)}$ of 400 K obtained using the OH ($A^2\Sigma^+$, $\nu = 0$) → OH($X^2\Pi$, $\nu' = 0$) transition [22].

Nozaki et al. have developed a diagnostic method based on the emission spectroscopy of a rotational band of CH (431.5 nm) to determine the gas temperature and confirmed that the rotational temperature showed fairly good sensitivity to background gas temperature [23]. Using this method they

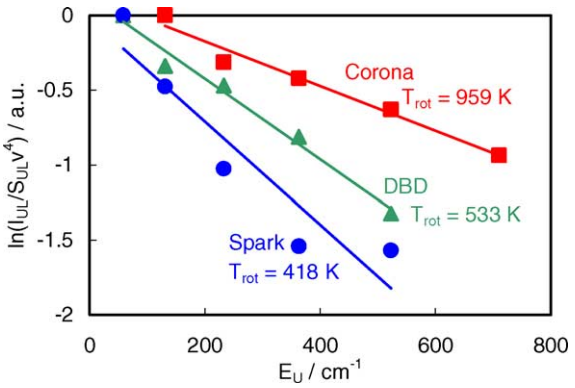

Fig. 8. Boltzmann plot obtained in DBD, corona and spark discharge and their estimated CH rotational temperature.

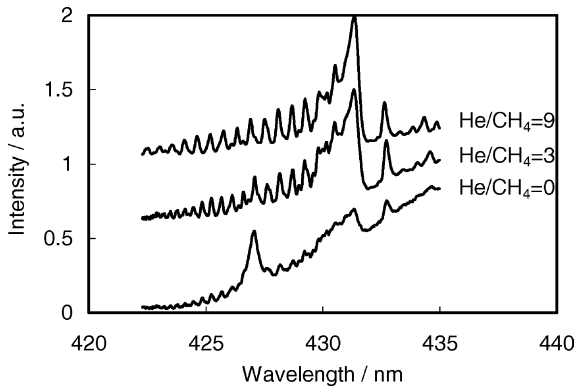

Fig. 9. Effect of He/CH_4 ratio on emission spectra of rotational band of CH in spark discharge.

have examined the energy distribution and thermal structure in DBD and APG (atmospheric pressure glow-discharge) [24,25].

In this study, the gas temperature was determined from CH rotational band in DBD, corona and spark discharge. Fig. 8 shows the Boltzmann plot obtained from the measured spectra versus the rotational energy of the levels in the upper state. The rotational temperature is calculated from the slope of straight line in Boltzmann plot. The rotational temperature in corona discharge was 959 K, which was much higher than that in DBD of 533 K. The high gas phase temperature in corona discharge caused the consecutive dehydrogenation as shown in Fig. 5.

Although the obtained rotational temperature in spark discharge was as low as 418 K, which was much lower than that of DBD and corona discharge, the reliability of this temperature was low because the Boltzmann plot did not agree with the approximate straight line. In addition, Yao et al. estimated that the gas temperature in spark discharge channel increased up to ca. 2340 K due to the Ohmic heating from the calculation. They assumed that there were no reactions and no energy and mass exchanges between gases inside and outside the channel.

The reasons why the Boltzmann plot in spark discharge did not give the straight line are: (1) weak emission intensity of CH rotational band, (2) disturbed R-branches of CH rotational band due to the strong emission from atomic carbon around 427 nm and (3) complex baseline due to broadened Hγ line (434 nm). Fig. 9 shows the spectra of CH rotational band and atomic carbon obtained in pure methane flow, and the effect of dilution with helium on spectra. It was found that the dilution of methane with helium resolved three problems mentioned above. The emission intensity of CH rotational band became stronger with the increase in helium concentration in the feed gas, and the reliable gas temperature was determined.

Fig. 10 shows the effect of He/CH_4 ratio of the feed gas on the rotational temperature. The rotational temperature increased with the increase in He/CH_4 ratio. In spark discharge, the width of pulsed current was 500 ns at most, which was much shorter than the interval between pulses of 20 ms. So, the increase in the temperature is considered to be caused by changes in the heat capacity of feed gas, and the effect of thermal conductivity can be neglected. And the relationship between discharge power and temperature can be written as the following equation, which was used by Yao et al. in their calculation [19]:

$$VI\,\mathrm{d}t = mC_p\,\mathrm{d}T$$

Here m (mol) is the total moles of feed gas in discharge channel and C_p (J K^{-1} mol^{-1}) is the heat capacity at constant pressure. The reciprocal of the average heat capacity ($1/C_p$) was also plotted with a solid line in Fig. 10. The rotational temperature and the reciprocal of the heat capacity showed the same behavior toward He/CH_4 ratio, and the gas temperature of 420–460 K in pure methane spark discharge is considered reasonable. This low gas phase temperature is favorable for quenching activated species and selective production of acetylene with small amount of deposited carbon [26].

3.5. Improvement of energy efficiency

To improve the energy efficiency for the production of acetylene and hydrogen with spark discharge, the

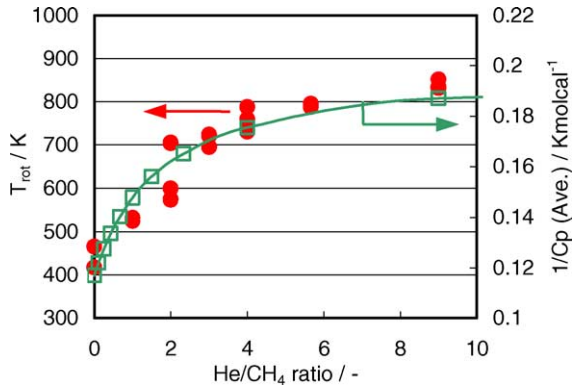

Fig. 10. Behavior of rotational temperature in spark discharge toward He/CH_4 ratio and its relationship with average heat capacity.

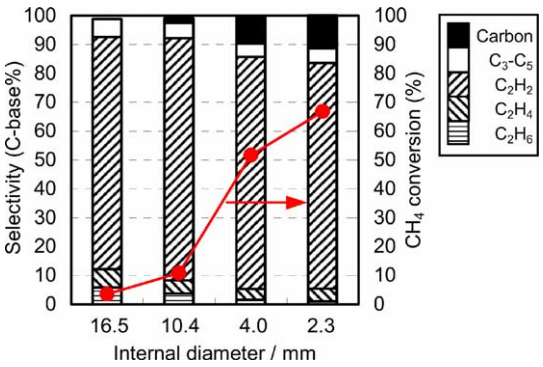

Fig. 11. Effect of internal diameter of reactor on reactivity of spark discharge in pure methane flow.

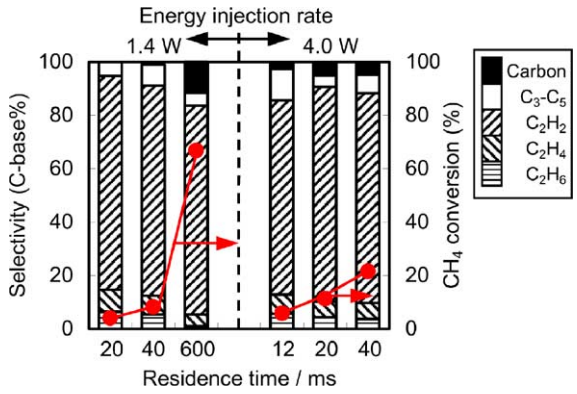

Fig. 13. Effect of residence time and energy injection rate on reactivity of spark discharge in pure methane flow (Ø2.3 mm i.d. reactor).

optimization of reaction conditions was examined besides the discharge conditions. The maximum diameter of the discharge channel was estimated to be ca. 0.9–1.3 mm from the image of spark discharge taken with an ultra-high-speed digital imaging system [19]. This indicated that most of methane might pass through the discharge region without contacting with the discharge channel.

Fig. 11 shows the effect of internal diameter of the reactor on the selectivity and conversion under the condition of the same residence time of 0.6 s. The residence time was determined from the reactor volume between the electrodes defined as a reaction volume. With the decrease in the internal diameter, methane conversion increased while the main product remained acetylene although the selectivity to carbon slightly increased. Fig. 12 shows methane conversion rate and specific energy requirement for C_2H_2. Methane conversion rate increased from 1.7 μmol/J (Ø16.5 mm) to 2.1 μmol/J (Ø10.4 mm), but decreased gradually with further decrease in the internal diameter of the reactor. The lowest specific energy requirement for C_2H_2 was 12.1 kW h/kg-C_2H_2 obtained with 10.4 mm i.d. reactor. The decrease in the energy efficiency with thin reactor tube was considered caused by high methane conversion, which led to low methane concentration and energy loss in the decomposition of products.

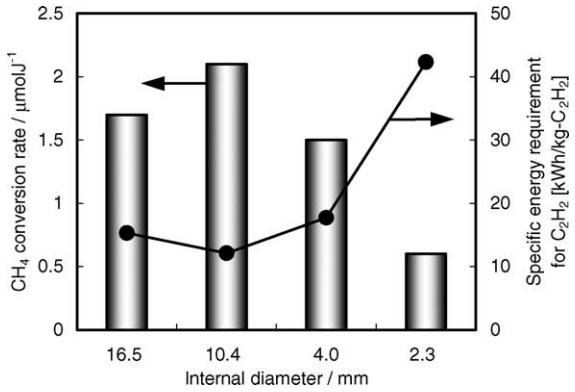

Fig. 12. Effect of internal diameter of reactor on energy efficiency.

Using Ø2.3 mm i.d. reactor, the effect of residence time was examined under the conditions of 1.4 and 4.0 W energy injection rate (Fig. 13). It was natural that longer residence time gave higher methane conversion at the same energy injection rate, and higher energy injection rate gave higher methane conversion at the same residence time without affecting the selectivity so much. From Fig. 14, too short and too long residence time was not favorable to efficient production of acetylene and hydrogen. There was an optimum condition in residence time, and in this case, it was 20 ms, which corresponded to pulse period. Under this condition, the reactant gas was replaced per pulse. The efficient feed of reactant and removal of products are necessary. And the necessity of the optimization of energy injection rate was indicated from the fact that higher energy injection rate increased the specific energy requirement for C_2H_2.

In addition, the specific energy requirement for C_2H_2 obtained with Ø2.3 mm i.d. reactor was higher than that obtained with Ø10.4 mm i.d. shown in Fig. 12. This indicates that the diffusion in the direction perpendicular to the discharge channel is also important. Fig. 15 shows the effect of residence time on specific energy requirement for C_2H_2 when Ø10.4 mm i.d. reactor was used. The lowest specific

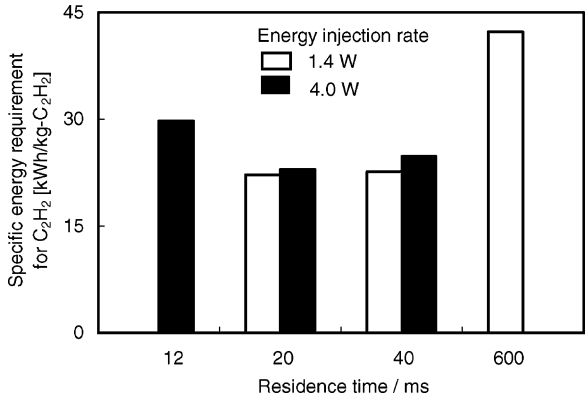

Fig. 14. Effect of residence time and energy injection rate on specific energy requirement for C_2H_2 (Ø2.3 mm i.d. reactor).

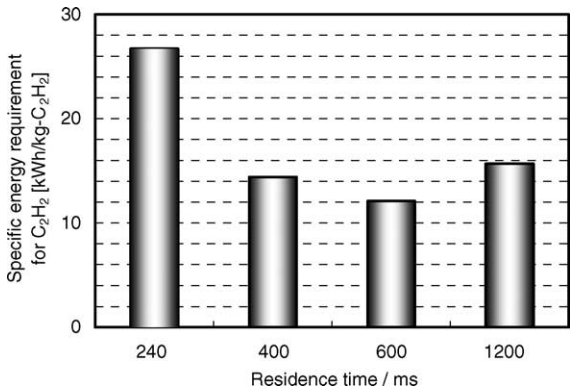

Fig. 15. Effect of residence time on specific energy requirement for C_2H_2 (Ø10.4 mm i.d. reactor).

energy requirement for C_2H_2 of 12.1 kW h/kg-C_2H_2 was obtained at 0.6 s residence time, which was much longer than pulse period. These experiments were conducted in pure methane flow with relatively large amount of deposited carbon, so it is possible that this energy cost will be improved by mixing moderate concentration of oxygen to prevent carbon deposition and enhance methane conversion [27].

The obtained energy cost of 12.1 kW h/kg-C_2H_2 is as same as that of Huels process, which was industrialized as acetylene plant using thermal plasma of DC arc discharge [28]. At this optimized condition, methane conversion rate and energy efficient were 2.1 μmol/J and 32.3%. Yao et al. used the similar reactor and achieved 2.73 μmol/J with high frequency pulsed discharge (9.92 kHz) [29]. They have reported that methane conversion rate increased with the increase in the pulse frequency, and our system showed much higher methane conversion rate as compared with their system at the same frequency as low as 50 Hz. It is also necessary to optimize the pulse frequency in our system.

Fig. 16 summarizes methane conversion of all experiments conducted in this study as a function of specific input energy (eV/molecule). The results of DBD and corona discharge were dotted on the same curve. On the other hand, methane conversions obtained in spark discharge were much higher than those of DBD and corona discharge at the same specific input energy. Even in spark discharge, the energy efficiency decreased drastically in the range of methane conversion higher than ca. 60%. In the pulsed microwave plasma, this problem was overcome and linear increase in methane conversion was observed up to 80% [18]. At this stage, our pulsed spark discharge has an advantage in relatively low energy injection rate.

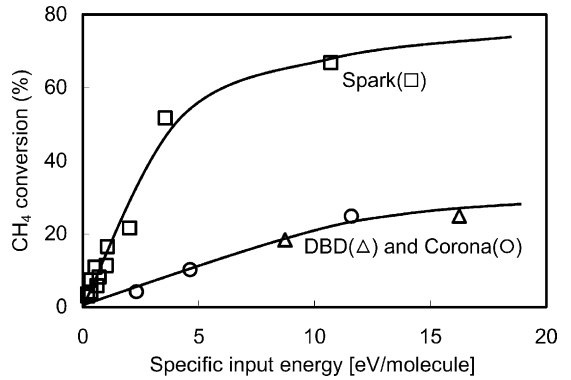

Fig. 16. Comparison of methane conversion among DBD, corona and spark discharge as a function of specific input energy.

4. Conclusion

Comparison of the properties among DBD, corona and spark discharge was made under the conditions of room temperature, atmospheric pressure and pure methane flow. The spark discharge showed much higher reactivity and selectivity to acetylene than those of DBD and corona discharge. From emission spectroscopic study, it was found that methane was highly dissociated to atomic carbon and hydrogen by the collision of electrons, and that the gas temperature in spark discharge channel was as low as 420–460 K, which indicated that the high selectivity to acetylene was not caused by thermal reaction. The highest energy efficiency of 32.3% for the production of acetylene was obtained by the optimization of reactor size and residence time. Under this condition, the specific energy requirement for acetylene was 12.1 kW h/kg-C_2H_2, which was as same as that in Huels process using DC arc plasma.

Acknowledgements

S. Kado is grateful for his Research Fellowship from the Japan Society for the Promotion of Science (JSPS) for Young Scientists. The authors greatly appreciate the intensive discussion with Professor Kazuyuki Tohji and Dr. Yoshinori Sato (Tohoku University) about the purification of carbon materials and Raman spectroscopy.

References

[1] O.V. Krylov, Catal. Today 18 (1993) 209.
[2] S. Kado, Y. Sekine, K. Fujimoto, Chem. Commun. 24 (1999) 2485.
[3] S. Kado, K. Urasaki, Y. Sekine, K. Fujimoto, Chem. Commun. 5 (2001) 415.
[4] S. Kado, K. Urasaki, H. Nakagawa, K. Miura, Y. Sekine, in: C.J. Liu, et al. (Eds.), Utilization of Greenhouse Gases, Proceedings of the ACS Symposium Series 852, 2003, p. 302.
[5] S. Kado, K. Urasaki, Y. Sekine, K. Fujimoto, Therm. Sci. Eng. 11 (2003) 1.
[6] T. Nozaki, Y. Kimura, K. Okazaki, J. Phys. D 35 (2002) 2779.
[7] D. Liu, S. Yu, T. Ma, Z. Song, X. Yang, Jpn. J. Appl. Phys. 39 (2000) 3359.
[8] C.J. Liu, Y. Li, Y.P. Zhang, Y. Wang, J.J. Zou, B. Eliasson, B.Z. Xue, Chem. Lett. 30 (2001) 1304.
[9] T. Jiang, Y. Li, C.J. Liu, G.H. Xu, B. Eliasson, B.Z. Xue, Catal. Today 72 (2002) 229.
[10] Y. Li, C.J. Liu, B. Eliasson, Y. Wang, Energy Fuels 16 (2002) 864.

[11] J.J. Zou, Y. Li, Y.P. Zhang, C.J. Liu, Acta. Physico-Chim. Sin. 18 (2002) 759.
[12] J.J. Zou, Y.P. Zhang, C.J. Liu, Y. Li, B. Eliasson, Plasma Chem. Plasma Process. 23 (2003) 69.
[13] H. Kabashima, S. Futamura, Chem. Lett. 31 (2002) 1108.
[14] J.Q. Zhang, J.S. Zhang, Y.J. Yang, Q. Liu, Energy Fuels 17 (2003) 54.
[15] J.Q. Zhang, Y.J. Yang, J.S. Zhang, Q. Liu, Acta. Chim. Sin. 60 (2002) 1973.
[16] K. Onoe, A. Fujie, T. Yamaguchi, Y. Hatano, Fuel 76 (1997) 281.
[17] M. Heintze, M. Magureau, J. Appl. Phys. 92 (2002) 2276.
[18] M. Heintze, M. Magureau, M. Kettlitz, J. Appl. Phys. 92 (2002) 7022.
[19] S.L. Yao, E. Suzuki, A. Nakayama, Plasma Chem. Plasma Process. 21 (2001) 651.
[20] K. Tohji, T. Goto, H. Takahashi, Y. Shinoda, N. Shimizu, B. Jeyadevan, I. Matsuoka, Y. Saito, A. Kasuya, T. Ohsuna, K. Hiraga, Y. Nishina, Nature 383 (1996) 679.
[21] K. Tohji, H. Takahashi, Y. Shinoda, N. Shimizu, B. Jeyadevan, I. Matsuoka, Y. Saito, A. Kasuya, S. Ito, Y. Nishina, J. Phys. Chem. B 101 (1997) 1974.
[22] S. Pellerin, K. Musiol, O. Motret, B. Pokrzywka, J. Chapelle, J. Phys. D 29 (1996) 2850.
[23] T. Nozaki, Y. Unno, Y. Miyazaki, K. Okazaki, J. Phys. D 34 (2001) 2504.
[24] T. Nozaki, Y. Miyazaki, Y. Unno, K. Okazaki, J. Phys. D 34 (2001) 3383.
[25] T. Nozaki, Y. Unno, K. Okazaki, Plasma Sour. Sci. Technol. 11 (2002) 431.
[26] R.P. Anderson, J.R. Fincke, C.E. Taylor, Fuel 81 (2002) 909.
[27] S. Kado, K. Urasaki, Y. Sekine, K. Fujimoto, Fuel 82 (2003) 1377.
[28] H. Gladisch, Hydrocarbon Process. Petrol. Refiner 41 (1962) 159.
[29] S.L. Yao, E. Suzuki, N. Meng, A. Nakayama, Plasma Chem. Plasma Process. 22 (2002) 225.